as 0.1 of one gland [approximately 50 ng of protein (*3*)] consistently exacerbated the course of cutaneous leishmaniasis to a degree equivalent to that obtained with 0.5 of one gland. Amounts less than 0.1 of one salivary gland had less effect in the system, but infection was enhanced later in the course of the disease. Sacks and Perkins (*6*) reported that developmental stages of *Leishmania* occur in the sand fly and result in the generation of highly infective parasites. Thus, vectorial capacity of a given phlebotomine species should be a reflection of the ability of the fly to generate infective forms of *Leishmania* and subsequently to enhance transmission of the parasite by means of the contents of the salivary gland.

REFERENCES AND NOTES

1. E. K. Markell and M. Voge, *Medical Parasitology* (Saunders, Philadelphia, 1971).
2. J. M. C. Ribeiro, *Annu. Rev. Entomol.* **32**, 463 (1987).
3. ———, P. A. Rossignol, A. Spielman, *Comp. Biochem. Physiol. A* **83**, 683 (1986).
4. R. Behin, J. Mauel, B. Sordat, *Exp. Parasitol.* **48**, 81 (1979); E. Handman, R. Ceredig, G. F. Mitchell, *Aust. J. Exp. Biol. Med. Sci.* **57**, 9 (1979).
5. R. G. Titus, M. Marchand, T. Boon, J. A. Louis, *Parasite Immunol.* **7**, 545 (1985).
6. D. L. Sacks and P. V. Perkins, *Science* **223**, 1417 (1984).
7. R. G. Titus, R. Ceredig, J.-C. Cerottini, J. A. Louis, *J. Immunol.* **135**, 2108 (1985).
8. G. B. Modi and R. B. Tesh, *J. Med. Entomol.* **20**, 568 (1983).
9. J. M. C. Ribeiro, J. J. F. Sarkis, P. A. Rossignol, A. Spielman, *Comp. Biochem. Physiol. B* **79**, 81 (1984).
10. J. M. C. Ribeiro and E. S. Garcia, *J. Insect Physiol.* **26**, 303 (1980).

11. Supported by NIH grants 1 R29 AI24511, AI18694 0481, and 5 P01 AI22794 and by the Rockefeller Foundation (RF85072 no. 125).

27 October 1987; accepted 20 January 1988

Neural Model of Adaptive Hand-Eye Coordination for Single Postures

MICHAEL KUPERSTEIN

A neural network model has been developed that achieves adaptive visual-motor coordination of a multijoint arm, without a teacher. The model learns to position an arm so that it reaches a cylinder arbitrarily positioned in space. The model uses a new neural architecture and a new algorithm for modifying neural-connection strengths. Computer simulations show that the model performs with an average position error of 4% of the arm's length and with an average orientation error of 4°. The model is designed to be generalized for coordinating any number of topographic sensory inputs with limbs of any number of joints.

THE HUMAN BRAIN DEVELOPS accurate sensorimotor coordination despite many unforeseen changes in the dimensions of the body, strength of the muscles, and placements of the sensory organs. This is accomplished for the most part without a teacher. How is this done? I present some new hypotheses and computer simulations of distributive neural representations and computations that suggest how at least one type of adaptive sensorimotor coordination might be developed and maintained. The hypotheses rely on the self-consistency between sensory and motor signals to achieve unsupervised learning. They also rely on the topography of units in a network. (Topography is the ordered contiguous representation of inputs or outputs across a surface with possible overlap of neighboring representations.) Topographic mappings have been found in most sensory and motor brain structures (*1*), and their computational properties are just beginning to be studied (*2*).

This study combines the constraints of self-consistency and topography toward the problem of adaptively coordinating a multijoint arm to reach a cylinder arbitrarily positioned in space, as viewed by two eyes.

Biology Department, Wellesley College, Wellesley, MA 02181.

The first hypothesis is that representations of postures emerge out of the correlation between posture sensation and target sensation. Such a correlation allows sensation and manipulation to become self-consistent. The self-consistency hypothesis is an extension of results from developmental studies in coordination behavior. Studies in the kitten (*3*) show that visually guided behavior develops only when changes in visual stimulation are systematically related to self-produced movement. The hypothesis is also consistent with the motor theory of speech perception (*4*).

The second hypothesis explores one of the ways a correlation between sensation and manipulation can be developed, called the circular reaction, which is an extension of one of Piaget's developmental stages (*5*). This reaction comes in two phases (Fig. 1). Self-produced motor signals are first generated to explore a large range of arm postures. During each posture, with object in hand, topographic sensory information about the object is projected to a target map through modifiable gating factors, called weights, which produce computed motor signals. Differences between the actual (self-produced) motor signals generated for each posture and the computed motor signals are used to change the weights so that these differences are minimized. These weight changes, for all possible motor postures, constitute the sensorimotor correlation and allow the system to become self-consistent. This is not simply feedback error correction. The weight changes must be structured in a way to allow global consistency for similar targets in all possible positions.

The second phase of the circular reaction takes effect after the correlation has been developed. In this phase, the self-consistency developed in the first phase is used to grasp objects found free in space. Sensory information about the object projects to a target map through the correlated weights and thereby evokes the appropriate motor signals to grasp that object.

The neural model of the circular reaction was implemented by means of discrete arithmetic and difference equations operating on matrices of numbers. The mechanical system that the model controls was rendered on a graphics workstation (Fig. 2).

Arm-muscle signals a_{pq} activate antagonistic muscle pairs ($p = 1,2$) in five degrees of freedom ($q = 1, \ldots, 5$) for the upper and lower limbs: shoulder roll ($q = 1$),

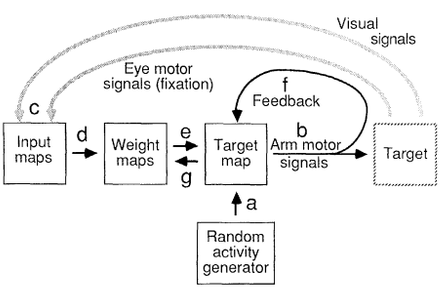

Fig. 1. The circular reaction. Self-produced motor signals that manipulate an object target are correlated with target sensation signals. The sequence for training is a, b, c, d, (e+f), g. Correlated learning is done in step g. After the correlation is achieved, target sensation signals alone can evoke the associated motor signals to accurately manipulate the target. The sequence for performance is c, d, e, b.

shoulder pitch ($q = 2$), shoulder yaw ($q = 3$), elbow roll ($q = 4$), and elbow yaw ($q = 5$). The neural model has no a priori knowledge of spatial relations of the mechanical system. The two-fingered hand is neither sensed nor controlled in the present neural model, although it could be.

The eye-muscle signals e_{pq} activate three pairs of antagonistic muscles ($p = 1,2$) for each eye that pull the eye in directions spaced 60° apart ($q = 1,2,3$). Each eye also registers a visual field matrix composed of light intensity v_{ij}, where $i = 1, \ldots, I$, $j = 1, \ldots, J$. The network operates over N learning trials. Figure 3 shows the neural networks for one typical trial.

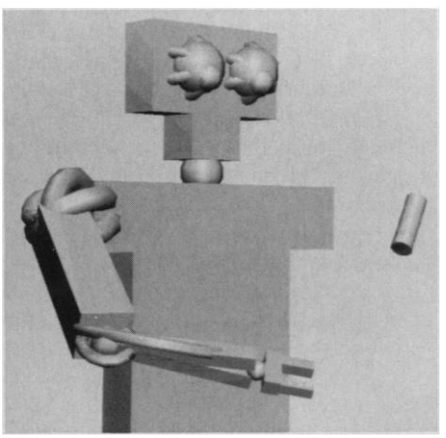

Fig. 2. Rendering of the mechanical system used for seeing and grasping as simulated on a graphics workstation. Each of two eyes moves in a pitch and yaw direction controlled by six muscles that pull in directions spaced 60° apart. Each eye senses a 50 by 50 matrix of binary visual intensity. The arm moves in five degrees of freedom controlled by five pairs of antagonistic muscles. The shoulder joint moves in pitch, yaw, and roll and the elbow joint moves in yaw and roll.

On trial n, the signals for the arm muscles are first randomly generated (*6*) and normalized. In the simplest case, the joint angle of the limbs is computed to be linearly proportional to muscle activation (*7*). However, any one of many monotonic functions of arm-muscle signals can be chosen with similar results. Activation of the arm muscles leads to an arm posture with the two-fingered hand initially holding a cylinder. The model is then told where to orient the two eyes so that they point toward the visual contrast center of the cylinder target. This information can also be obtained by another adaptive neural model used to control eye foveation (*8*) without changing the present results. The eye foveation model uses the same neural architecture and was designed to work in parallel with the present model.

The eye-muscle signals e_{pq} that correspond to the eye orientations are then used as input to the network. These signals are transformed into unimodal distributions of activity $E^{l}_{pq\langle i\rangle}$ (left) and $E^{r}_{pq\langle i\rangle}$ (right) across networks of units ($i = 1, \ldots, I$). Each distribution represents a topography for each eye-muscle signal. Any one of a large family of transformations can be chosen without affecting the results. The main criterion for these transformations is that the positions of unimodal distribution peaks vary monotonically with eye-muscle signal.

For the present model a transformation was chosen that mimics realistic neural responses in the oculomotor nuclei of the brain (*9*). It is called the "recruitment" function because it recruits increasingly more neural elements with increasing muscle signal amplitude (*10*). In this case

$$E_{pq\langle i\rangle} = \max\{0, f(i)[e_{pq} - g(i)]\} \quad (1)$$

where $f(i) = \alpha i/I$; $g(i) = \beta i/I$; $i = 1, \ldots, I$; and α, β are constants.

To make use of binocular information, the model combines the left and right eye-muscle distributions $E^{l}_{pq\langle i\rangle}$ and $E^{r}_{pq\langle i\rangle}$ to form a topographic disparity distribution $E^{d}_{pq\langle i\rangle}$. This distribution has the following properties: (i) it describes a measure of disparity between eye orientations; (ii) it has a topography across orientation space; (iii) the computation does not depend on which of the two eye orientations is larger (symmetry); and (iv) both eyes must be active for the disparity to be computed (binocularity). One simple function, of many, that satisifies these constraints for the disparity distribution is

$$E^{d}_{pq\langle i\rangle} = \lambda E^{l}_{pq\langle i\rangle} E^{r}_{pq\langle i\rangle} \mid E^{l}_{pq\langle i\rangle} - E^{r}_{pq\langle i\rangle} \mid \quad (2)$$

where λ is a constant and $i = 1, \ldots, I$ (network population). The distributions $E^{l}_{pq\langle i\rangle}$,

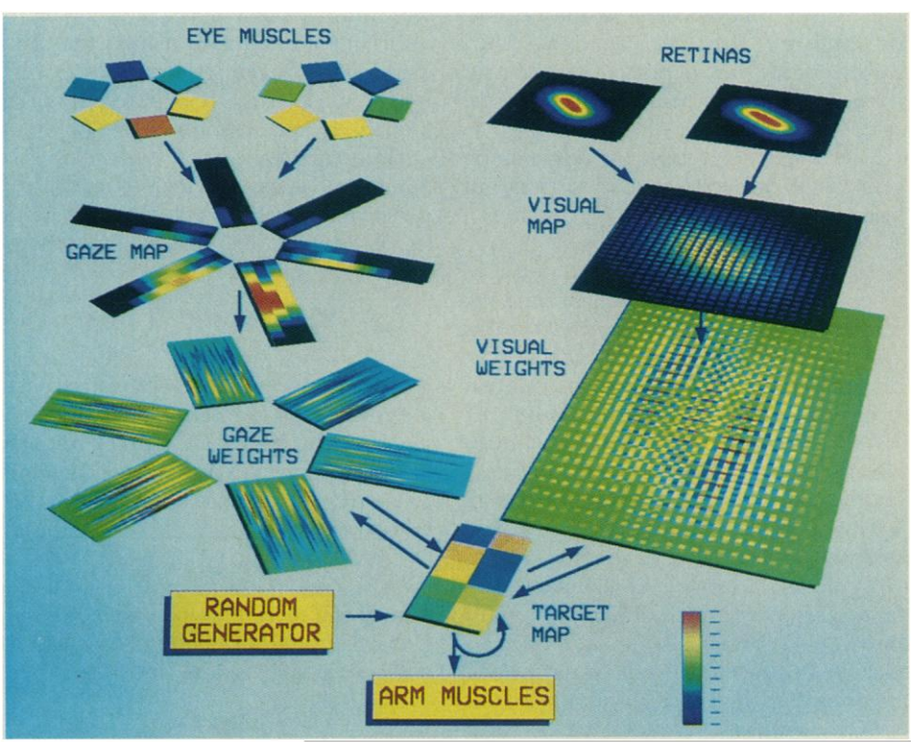

Fig. 3. The neural model in a typical learning trial. The relative values of neural signals are shown as colors across the surfaces of the neural networks, according to the scale at the bottom. During learning, the random generator first produces signals that position the arm in some posture, while the hand holds a cylinder. Then the two eyes orient to the cylinder. The eye-muscle signals are transformed into a gaze map that contains information about the directions of gaze of the eyes and their disparities. Each leg of the gaze map represents the pulling direction on either eye. The amplitudes of the three eye-muscle distributions (left-eye, disparity, and right-eye) are shown by the colors along the map's radii (100 units in each of 18 distributions). The gaze weights (18,000 values) contain gating signals from each gaze map unit to each arm-muscle unit. A similar series of transformations occur for visual signals. First, stereo views of the grasped cylinder are registered in the retinas (50 by 50 units each). In each trial, these images are processed for contrast orientation and binocular disparity. The visual map shows interleaved orientation and disparity responses from both eyes. The visual weights contain gating signals from each visual map unit to each arm-muscle unit. (Only 6.7% of the 300,000 visual weights are shown for clarity.) Arm-muscle signals are produced by normalizing the sum of the products of both the gaze map and visual map with their respective weight maps. These signals are compared against arm-muscle signals produced by the random generator. The differences are used to change values in the two weight maps so that on future trials the differences will be minimized.

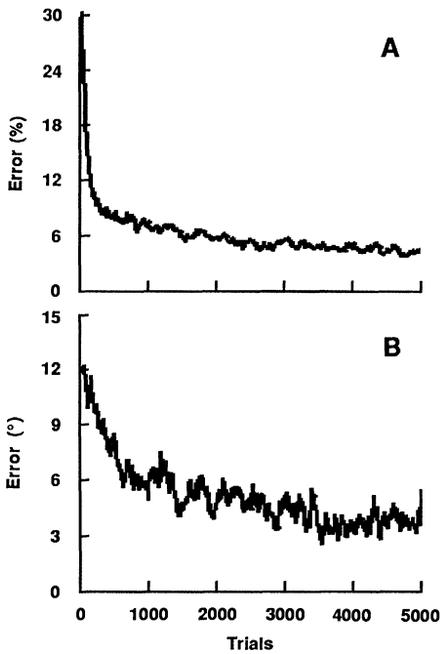

Fig. 4. Convergence of (**A**) the average position errors and (**B**) the orientation errors for grasping a cylinder that is positioned randomly in space.

$E^{r}_{pq\langle i\rangle}$, and $E^{d}_{pq\langle i\rangle}$ together comprise the gaze map.

Each eye also receives a two-dimensional visual projection of the cylinder target in space, called a retinal map, v. Stereo maps, each of which is composed of binary light intensity distributions, are processed for graded contrast orientation in four directions, x: 0°, 45°, 90°, and 135°. The resulting transformations comprise the orientation maps $V^{l}_{x\langle ij\rangle}$ (left) and $V^{r}_{x\langle ij\rangle}$ (right). Then corresponding pairs of orientation maps are combined into binocular-disparity maps, $V^{d}_{x\langle ij\rangle}$.

The orientation maps are achieved by convolving each retinal map v_{ij} with an orientation kernel k_x

$$V_{x\langle ij\rangle} = v_{\langle ij\rangle} * k_x \qquad (3)$$

where k_x are kernel matrices that have the same nonpositive coefficients everywhere except along one string in one of the four orientations, x. The coefficients in that string are all the same positive number.

The responses of the orientation maps mimic the orientation responses of visual cortex neurons to visual contrast (*11*). Other orientation-response functions can be used with similar results.

By means of a disparity computation similar to one for eye-muscle disparity, the visual disparity distributions $V^{d}_{x\langle ij\rangle}$, are formed by combining pairs of corresponding orientation distributions in the function

$$V^{d}_{x\langle ij\rangle} = \delta\, V^{l}_{x\langle ij\rangle} V^{r}_{x\langle ij\rangle} \mid V^{l}_{x\langle ij\rangle} - V^{r}_{x\langle ij\rangle} \mid \qquad (4)$$

where δ is a constant. This response is similar to the disparity response of binocular neurons in the visual cortex (*12*). When all the V distributions are interleaved (Fig. 3) they form the visual map, which mimics the retinotopic layout of some of the neural responses observed in the visual cortex (*13*).

Next, the gaze map and the visual map are combined to produce arm-muscle signals through their respective weight maps. The modifiable weights (Fig. 3) in these maps act as gates between sensation and posture. The weights are changed by a learning rule during each trial, which develops the correlation between topographic sensory signals and topographic motor signals across all trials.

The architecture of the weight maps is crucial to the performance of the neural model. It is composed of distributed, interleaved combinations of topographic sensory inputs that are transformed into a distributed, interleaved combination of motor outputs. The interleaving arrangement is noted by the expression $ij\langle pq\rangle$, which means map position i,j composed of a distribution of limb-muscle elements p,q. The product of the input maps and their respective weight maps are disentangled and converged to separate arm-muscle outputs and constitute the computed motor signals M'_{pq}

$$M'_{pq} = \sum_{ij} (S_{ij}\, W_{ij\langle pq\rangle}) \qquad (5)$$

where S_{ij} is every input element from both the gaze map and the visual map and the $W_{ij\langle pq\rangle}$ are the modifiable weights. In essence, each input element is connected to each limb-muscle representation through a modifiable weight element. Note that weight values $W_{ij\langle pq\rangle}$ can be negative. All weights are initialized to 0.

These computed motor signals are then normalized across antagonistic muscle pair representations along with the actual motor signals (random values), M_{pq} to produce arm-muscle signals (*14*):

$$a_{pq} = (M_{pq} + M'_{pq}) / \sum_{p} (M_{pq} + M'_{pq}) \qquad (6)$$

The model develops self-consistency and improves its performance by modifying the target weights $W_{ij\langle pq\rangle}$. The learning rule minimizes the difference between the computed and actual motor signals. Thus, the differences or errors ε_{pq} are

$$\varepsilon_{pq} = M_{pq} - M'_{pq} \qquad (7)$$

Minimizing these differences while allowing global convergence requires changing all active weights by a small amount

$$W_{(n+1)ij\langle pq\rangle} = W_{(n)ij\langle pq\rangle} + \sigma S_{ij} \varepsilon_{pq} \qquad (8)$$

where n is the trial number and σ is the learning rate. The learning rule states that the target weights (corresponding to those sensory inputs that are active) are changed by an increment that depends on the component of an error in the respective muscle direction (*15*). This component-specific learning occurs back in the weight maps. With this incremental learning rule, the computed motor signals for all targets converge towards the actual motor signals (ε_{pq} is minimized) in successive trials.

When learning converges, the model can accurately control the reaching postures to cylinders found free in space. In this phase, the eyes first orient toward the cylinder target. The target is sensed by the sensory maps, which in turn produce computed motor signals through the accumulated weights. In this condition the random signal generator is off ($M_{pq} = 0$ in Eq. 6). When these values are used to control arm posture, the end of the arm reaches the cylinder target because the weight maps have developed a correlation between the sensory maps and the arm-muscle signals.

The objective accuracy of the model's performance (not known to the model) is determined by averaging the differences between the actual target positions and the computed arm positions in Cartesian coordinates for all trials. Computer simulations show that, throughout the continuous volume of the available grasping space, the model performs with an average position error of 4% of the arm's length and an average orientation error of 4°. Learning converges in about 3000 to 5000 trials (Fig. 4). Learning rates σ (in Eq. 8) are in the range of 10^{-4} to 10^{-3}.

The model is designed to maintain adaptation when unforeseen changes are made in the mechanical system or with partial damage to the model, as was shown for the first prototype of the neural architecture used in this model (*16*). This study shows that the same neural architecture can be used for multiple topographic inputs from different modalities to achieve self-consistency. I suggest that, in general, adaptive topographic mapping constrained by self-consistency allows representations of objects by means of signals derived only from sensory receptors and motor feedback. No a priori knowledge of objective features is required.

REFERENCES AND NOTES

1. E. R. Kandel and J. H. Schwartz, *Principles of Neural Science* (Elsevier, New York, 1985).
2. S. Grossberg and M. Kuperstein, *Neural Dynamics of Adaptive Sensory-motor Control: Ballistic Eye Movements* (Elsevier, Amsterdam, 1986); E. I. Knudsen *et al. Annu. Rev. Neurosci.* **10**, 41 (1987); E. Schwartz, in *Proceedings of the First International Conference on Neural Nets*, San Diego, June 1987 (Computer Society Press, Washington, DC, 1987), p. 1595.
3. R. Held and A. Hine, *J. Comp. Physiol. Psychol.* **56**, 872 (1963).

4. H. Williams, and F. Nottebohm, *Science* **229**, 279 (1985); A. M. Liberman *et al.*, *Psychol. Rev.* **74**, 431 (1967).
5. J. Piaget, *The Origins of Intelligence in Children*, translated by M. Cook (International University Press, New York, 1952).
6. The degree of flatness of the random function has no bearing on the results. The range is 0 to 1.
7. This is formally shown in Eq. 6 and discussed there.
8. See M. Kuperstein [*Behav. Neurosci.* **102**, 148 (1988)] for adaptive neural architecture for eye foveation and first reference in (*2*) for eye movement generator.
9. E. S. Luschei and A. F. Fuchs, *J. Neurophysiol.* **35**, 445 (1972); D. A. Robinson, *ibid.* **33**, 393 (1972); P. H. Schiller, *Exp. Brain Res.* **10**, 347 (1970).
10. The recruitment function is the same as the position-threshold-slope function from the first reference in (*2*).
11. D. H. Hubel and T. N. Wiesel *J. Physiol. (London)* **195**, 215 (1968).
12. G. F. Poggio and B. Fischer, *J. Neurophysiol.* **40**, 1369 (1977).
13. D. Rose and V. G. Dobson, Eds., *Models of Visual Cortex* (Wiley, Chichester, U.K., 1985).
14. Normalized networks that have this property are similar to those used in S. Grossberg, *Studies of Mind and Brain* (Reidel, Dordrecht, 1982).
15. The present learning rule contrasts with a learning rule based on sensory errors [such as those used in (*8*)]. Unlike the former rule, the latter requires error directions to be calibrated a priori. Unlike the latter rule, the former requires exploratory motor signals to be generated. The use of each type of rule depends on the cost-benefit of their properties. They could also be used in parallel.
16. M. Kuperstein, in *Proc. IEEE Int. Conf. Automat. Robotics*, Raleigh, NC, 31 March to 3 April 1987 (Computer Society Press, Washington, DC, 1987), p. 1595.
17. I thank the National Science Foundation and the Air Force Office of Scientific Research for their financial support of this research (grant DMC-8521535).

2 November 1987; accepted 20 January 1988

Gene Encoding the β Subunit of S100 Protein Is on Chromosome 21: Implications for Down Syndrome

R. ALLORE, D. O'HANLON, R. PRICE, K. NEILSON, H. F. WILLARD, D. R. COX, A. MARKS, R. J. DUNN

S100 protein is a calcium-binding protein found predominantly in the vertebrate nervous system. Genomic and complementary DNA probes were used in conjunction with a panel of rodent-human somatic cell hybrids to assign the gene for the β subunit of S100 protein to the distal half of the long arm of human chromosome 21. This gene was identified as a candidate sequence which, when expressed in the trisomic state, may underlie the neurologic disturbances in Down syndrome.

DOWN SYNDROME (DS) IS THE most common genetic cause of human mental retardation, occurring with the frequency of about 1 per 800 live births (*1*). Individuals with this disorder have abnormalities in a number of different organ systems including the nervous system. Neuropathological changes consisting of neurofibrillary tangles, senile plaques, and neuronal loss are found in the brains of most DS individuals dying after the age of 35 years. These changes, which are qualitatively and quantitatively indistinguishable from those seen in Alzheimer's disease (AD), are often associated with the clinical features of presenile dementia (*2*). Cytogenetic studies have shown that a chromosome abnormality, trisomy of chromosome 21, is the primary cause of DS. This finding suggests that the neurologic abnormalities in DS are due to imbalance of one or more genes on chromosome 21. In order to understand the biochemical basis of the neurologic defects in DS it is necessary to identify these genes.

Two genes that may play a role in the neurologic abnormalities that characterize DS have recently been assigned to human chromosome 21 (*3, 4*). The first of these is the locus coding for amyloid β protein (APP), an important component of both cerebral vascular amyloid and amyloid plaques of AD and DS. The second gene, mutations of which result in early onset familial AD (which is autosomal-dominant), has been shown to be tightly linked to the chromosome 21 DNA marker, D21S16. Although both D21S16 and APP have been physically assigned to the proximal portion of the long arm of chromosome 21, crossovers between APP and the familial AD gene indicate that these are two separate loci (*5, 6*). We now report that a third gene, expressed primarily in the nervous system and encoding the β subunit of the S100 protein, maps to the distal half of the long arm of human chromosome 21 and is a candidate for the primary defect underlying the neurologic disturbances found in DS.

S100 protein is a calcium-binding protein widely distributed in the nervous system of vertebrates (*7*). It is structurally similar in the calcium-binding domains to calmodulin, an important transducer of calcium-mediated signals (*8*). S100 protein is composed of two subunits, α and β, which associate into αα, ββ, or αβ dimers (*9*). The highest levels of S100 protein are found in the brain. In particular, the β subunit of S100 protein is expressed in glial cells at levels at least tenfold higher than in most other cell types. The brain also contains small amounts of the α subunit at levels approximately one-tenth that of the β subunit (*10*). S100 protein accumulates during the maturation of the mammalian brain (*11*) and participates in several calcium-dependent interactions with neuroleptic drugs and brain proteins (*12*). Thus disturbances of S100 protein gene expression may play a fundamental role in the generation of neurologic defects associated with DS.

The human genomic and complementary DNA (cDNA) probes used to identify the chromosomal location of the S100 protein β subunit gene are shown in Fig. 1. The 742-

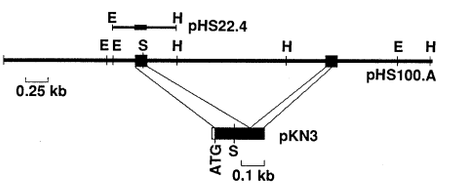

Fig. 1. Schematic representation of the genomic clone (pHS100.A), the genomic probe subclone (pHS22.4), and the cDNA clone probe (pKN3) used for Southern blot analysis. Protein coding region sequences are indicated by dark boxes. The heavy line indicates intron sequence in the genomic clone and the open box indicates the 5′ untranslated region sequence within the cDNA clone. Lines joining regions of cDNA and genomic clones bracket areas of identical sequence. The location of the ATG initiation codon is indicated. The DNA fragment used as a genomic hybridization probe (pHS22.4) is indicated above the genomic clone (pHS100.A) diagram. The cDNA clone was isolated by means of a previously characterized cDNA clone of the rat S100 protein β subunit (*17*), which was used as a hybridization probe. The Eco RI fragments from positive cDNA clones were subcloned into the Bluescript plasmid (Stratagene Cloning Systems, San Diego, CA). The genomic clone λHS100.1 was isolated by screening 3.6×10^5 recombinants from a λ Charon 4A human genomic library using the rat S100 protein cDNA probe (*18*). The 5.0-kb pHS100.A subclone of λHS100.1 contains the entire protein coding region from the S100 protein β subunit gene. The 0.746-kb genomic clone (pHS22.4) represents a 5′-coding region subclone from pHS100.A. Restriction enzyme sites: E, Eco RI; H, Hind III, and S, Sst I.

R. Allore, K. Neilson, H. F. Willard, R. J. Dunn, Department of Medical Genetics, University of Toronto, Toronto, Ontario, Canada M5S 1A8.
D. O'Hanlon and A. Marks, Banting and Best Department of Medical Research, University of Toronto, 112 College Street, Toronto, Ontario, Canada M5G 1L6.
R. Price and D. R. Cox, Department of Pediatrics, Biochemistry and Biophysics, M650, University of California, San Francisco, CA 94143.